X-ray irradiation effects on SH-SY5Y human neuroblastoma cells monitored by means of FTIR micro-spectroscopy

Valerio Ricciardi, Marianna Portaccio, Lorenzo Manti, Maria Lepore

Valerio Ricciardi, Marianna Portaccio, Lorenzo Manti, Maria Lepore, "X-ray irradiation effects on SH-SY5Y human neuroblastoma cells monitored by means of FTIR micro-spectroscopy," Proc. SPIE 11073, Clinical and Preclinical Optical Diagnostics II, 110731M (19 July 2019); doi: 10.1117/12.2526399

SPIE.

Event: European Conferences on Biomedical Optics, 2019, Munich, Germany

X-ray irradiation effects on SH-SY5Y human neuroblastoma cells monitored by means of FTIR micro-spectroscopy.

Valerio Ricciardi[a,b*#], Marianna Portaccio[a], Lorenzo Manti[b,c], Maria Lepore[a]
[a]Università della Campania "Luigi Vanvitelli", Dipartimento di Medicina Sperimentale, Via Santa Maria di Costantinopoli 16, 80138 Napoli (NA), Italy; [b]Istituto Nazionale di Fisica Nucleare - sezione di Napoli, Strada Comunale Cinthia, 80126 Napoli (NA), Italy; [c]Università degli Studi di Napoli "Federico II", Dipartimento di Fisica "E. Pancini", Via Cinthia, 80126 Fuorigrotta, Napoli (NA), Italy;

ABSTRACT

Fourier-Transform Infrared micro-spectroscopy (μFT-IR) was used for an in vitro investigation targeted to examine the effects on SH-SY5Y human neuroblastoma cells of X-rays irradiation. μFT-IR thanks to its ability in analyzing cells at a molecular level can be particularly useful in investigating the biochemical changes induced in protein, nucleic acid, lipid, and carbohydrate content of cells after irradiation by graded X-ray doses (0, 2, 4, 6, 8 and 10 Gy). Cell samples were fixed immediately (t0-cells) or 24h after (t24-cells) irradiation. A deconvolution procedure using Lorentzian curves was used for analyzing the collected spectra in order to highlight the changes due to the different treatment. Significant differences were evidenced in spectra from unexposed and exposed cells. Peaks related to important cell components (as Amide and DNA) show significant shifts depending on radiation dose and also the ratios between the intensity of selected bands are affected by the interaction with ionizing radiation. These changes are less evident in t24h-cells, thus suggesting the occurrence of repairing processes of the X-ray induced damage. The results of the present analysis can be helpful in order to develop innovative approaches to monitor radiation cancer radiotherapy outcome so as to reduce the overall radiation dose and minimize damage to the surrounding healthy cells, both aspects being of great importance in the field of radiation therapy.

Keywords: Fourier-Transform Infrared micro-spectroscopy, SH-SY5Y human neuroblastoma cells, X-ray effects on DNA, lipids, proteins and carbohydrates.

1. INTRODUCTION

Radiotherapy is largely used for tumor medical treatment in order to destroy neoplastic cells or proliferating ones. There is a large interest in researching on radiation interactions with cells and tissues for gaining better information on important radio-biological topics such as patient radio-sensitivity, monitoring patient's radio-response during treatment, and the inadequacy of available models to predict cell survival or tumor control at single high doses. Vibrational techniques such as Raman microspectroscopy and Fourier Transform Infrared microspectroscopy (μFTIR) [1-5] which can rapidly and non-invasively measure the spatially resolved chemistry of the cell and of tissue with minimal sample preparation, are attracting a growing interest importance in the field of radiation-induced cyto- and genotoxicity. Those techniques can be particularly useful in investigating the chemical changes induced in structure, protein, nucleic acid, lipid, and carbohydrate content of cells by means of radiation exposure.
In the last years, several researchers have adopted Fourier Transform Infrared microspectroscopy (μFT-IR) for the analysis of cell components, tissue sections and cell culture and for the investigation of different types of cancer and leukemia. All these studies suggest that infrared microscopy can be a valuable tool for monitoring the biomedical changes associated with the disease state [6]. In particular, μFT-IR has been proven to be useful in the analysis of the complex biological processes, including proliferation and cell death process, occurring during radiation-cell interaction [7, 8].

*valerio.ricciardi@unicampania.it; phone 39 348 835 8494; # Present address: Università della Campania "Luigi Vanvitelli", Dipartimento di Matematica e Fisica, Caserta, Italy

Clinical and Preclinical Optical Diagnostics II, edited by J. Quincy Brown, Ton G. van Leeuwen,
Proc. of SPIE-OSA, SPIE Vol. 11073, 110731M · © 2019 SPIE-OSA
CCC code: 1605-7422/19/$21 · doi: 10.1117/12.2526399

In the present work, μFT-IR spectroscopic analysis was performed on in vitro human SH-SY5Y neuroblastoma cells, irradiated with doses up to 10 Gy and subsequently subjected to a chemical fixing process that preserves cells during transport and measurements. Sample fixed immediately after (t_0-cells) and 24 h after irradiation ($_{t24}$h-cells) were prepared to study both the effects of the irradiation and the efficacy of the recovery process of the cells; this approach can offer a very direct way to monitor changes for specific cellular components.
SH-SY5Y cell line was chosen because it is one of the most common cancer in infants. Moreover, it is particularly relevant in neuroprotection studies aimed to develop new tools for the treatment and/or prevention of central nervous system disorders [9, 10].

2. MATERIALS AND METHODS

2.1 Cell sample preparations and treatments

The cell line used in this study is the SH-SY5Y neuroblastoma (American Type Culture Collection, Manassas, VA, USA), a human cell line subcloned from a bone marrow biopsy taken from a four-year-old female with neuroblastoma. The cells were grown at 37°, 5% CO_2 on MirrIR slide (25x25 mm^2) (Kevley Technologies, Chesterland, Ohio), a specific reflection FT-IR spectroscopy microscope slide with a cell surface density equal to $\sigma \approx 10000$ cells/cm^2). This cell density was chosen because it guarantees both presence of inter-cell space for the measurement of the background both the presence of clusters of cells necessary to obtain a sufficiently intense signal.
A STABILIPAN machine (Siemens, Munich, Germany) was used for X-ray irradiation (250 kVp, 1-mm Cu filter). Cellular samples derived from one single batch, in order to avoid inter-batch variation, were exposed to various dose of X-rays at a dose rate of 0.95 Gy/min. Cells exposed to 2, 4, 6, 8 and 10 Gy were investigated together with non-exposed cells (0 Gy). After the exposure, a set of cells was immediately fixed in 3.7 % paraformaldehyde while another set, maintained in the culture medium at 37°, 5% CO_2, was allowed to recover for 24 h after the exposure and then fixed; every sample was prepared in triplicate. Then the μFT-IR samples were dried under ambient conditions and stored in a desiccator until analysis (due to strong water molecules IR signal the humidity of the samples must be kept under control). These type of fixing procedures preserves the biochemical properties of the cells in the transport and during the measurement phase.

2.2 Spectra acquisition and data analysis

IR absorption spectra of the cell samples were acquired with a Spectrum One FTIR (PerkinElmer, Shelton, Connecticut) spectrometer equipped with a Perkin Elmer Multiscope system infrared microscope and an MCT (mercury cadmium telluride) FPA (focal-plane-array) detector. The measurements were performed on cells adherent on MirrIR slides having an area of 25x25 mm^2 in transflection mode. Every slide was examined in different regions and multiple spectra were acquired for each position. The measurements were made at room temperature by collecting the signal in the spectral region between 3600 and 900 cm^{-1} (64 scans, spectral resolution = 4 cm^{-1}, 5 s acquisition time for each spectrum). Subtraction of background spectrum, acquired in a free cells zone of the slide was performed. Average spectra with SD were obtained for all sample types. The spectra were further analyzed in terms of convoluted peak functions to determine the basic vibrational modes that contribute to the FT-IR signal by using a best-fit peak fitting routine based on the Levenberg-Marquardt nonlinear least-square method; Lorentzian curves were used. The best-fit was then performed to determine the optimized intensity, position, and width of the peaks using Lorentzian curves. The ratios between the intensity of selected bands was also evaluated (see Ref. 11 for a list of the evaluated ratio). Moreover, the band of Amide I was analyzed in details since significant variations were expected due to protein configuration changes. To determine protein secondary structure, the amide I band was deconvoluted by fitting it with Gaussian-Lorentzian cross product functions after localization of the minima in the second derivative spectrum. The area of each absorption band was assumed to be proportional to the relative amount of the structure type in infrared spectra [11-13].

3 RESULTS AND DISCUSSIONS

3.1 Control sample

In figure 1 the average FT-IR spectra of control cells (0 Gy, t = 0 h) is reported; the spectra presents different peaks divided into two zones: the fingerprint region (2000-800 cm^{-1}) and the high-wavenumber region (3600-2600 cm^{-1}).

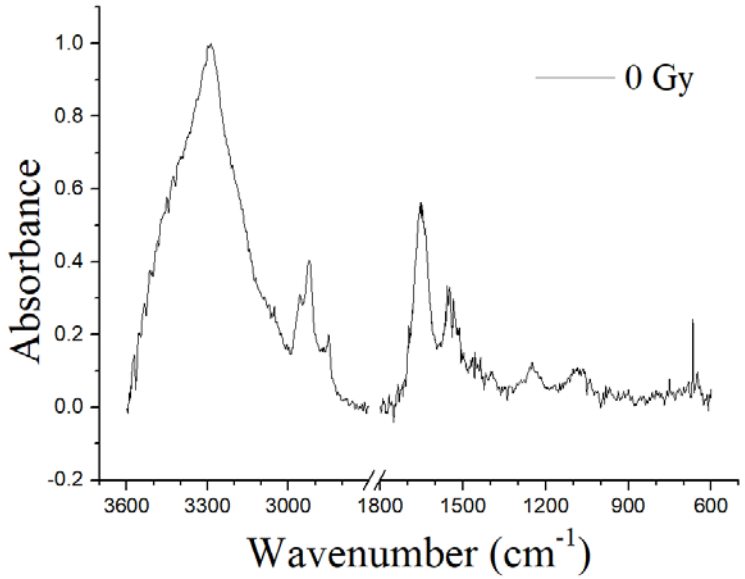

Figure 1. FTIR average absorbance spectrum in the range [3600-600 cm^{-1}] obtained from cells of the control sample, the break at [2700 – 1800 cm^{-1}] hides a region without interesting signals from biological molecules.

In the fingerprint region (2000-800 cm^{-1}, Figure 2A) different peaks, representative primarily, of proteins and nucleic acids are clearly visible. In particular, the two strong bands centred at ≈ 1650 cm^{-1} and ≈ 1540 cm^{-1} were mainly attributed to the Amide I (C = O and -C - N) and Amide II (N - H and C - N) stretching and bending of proteins. The band at ≈ 1450 cm^{-1} were due to symmetric and asymmetric bending of the methylene groups (CH_2 and CH_3) of lipids and the peak at ≈ 1400 cm^{-1} is assigned to COO^- groups asymmetric stretching of proteins and lipids. The two bands at ≈ 1240 cm^{-1} and ≈ 1085 cm^{-1}, respectively, included the asymmetric and symmetric -PO_2 stretching vibrations of the phosphodiester nucleic acid backbone.

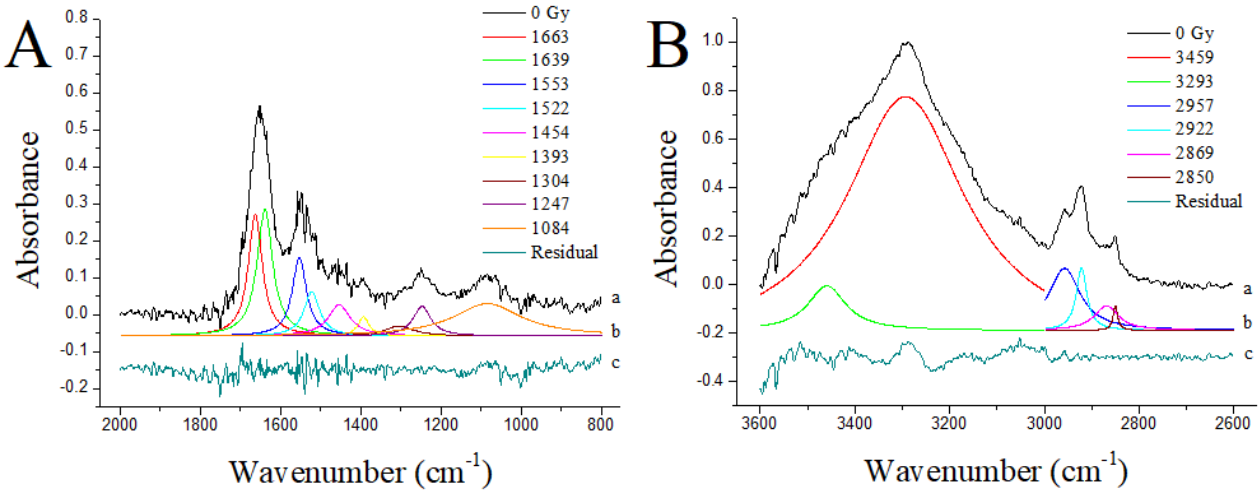

Figure 2. Spectra of one non exposed sample (A) in the range (2000-800 cm^{-1}) and (B) (3600-2600 cm^{-1}) (**a**) with deconvolution analysis of peaks with Lorentzian curves (**b**) and fit residual (**c**).

The region between (2600-2000 cm^{-1}) not shown signals by biological molecules while the high-wavenumber region (HWR) from (3600-2600 cm^{-1}, Figure 2B) shown characteristic bands associated mainly to proteins and lipids; in particular the bands in the range 3100 - 3500 cm^{-1} were attributed to the Amide A (N - H) stretching motion of peptide backbones of proteins amino acids, the peaks observed at ≈ 2960 cm^{-1} and ≈ 2870 cm^{-1} were assigned respectively to the asymmetric and symmetric stretching of the methyl groups (CH_3) arising from cellular proteins and lipids, and the bands

at ≈ 2920 cm^{-1} and ≈ 2850 cm^{-1} were assigned respectively to the asymmetric and symmetric stretching of the methylene groups of membrane lipids (CH_2).

A deconvolution analysis of the peaks in the two regions, (2000-800 cm^{-1}) (Figure 2.A) and (3600-2600 cm^{-1}) (Figure 2.B) of the average spectra of the control samples allowed the identification of other contribution from molecular groups present in biomolecules; in Table 1 the assignments for the resolved peaks are reported.

Table 1. FTIR peaks observed in the average spectrum of control cells, with assignments in accordance with the data reported in literature [1, 7, 14-16]; abbreviation: s = symmetric, as = asymmetric, ν = stretching, δ = bending, ς = scissoring.

Peak	**Assignment**		
cm^{-1}	DNA/RNA	Protein	Lipids
3293		$Amide\ A\ (N-H\ \nu)$	
2957		$CH_3\ as\ \nu$	$CH_3\ as\ \nu$
2922			$CH_2\ as\ \nu$
2869		$CH_3\ s\ \nu$	$CH_3\ s\ \nu$
2850			$CH_2\ s\ \nu$
1663		$Amide\ I\ (\alpha-helix)$	
1639		$Amide\ II\ (\beta-sheets)$	
1553		$Amide\ II\ (\alpha-helix)$	
1522		$Amide\ II\ (\beta-sheets)$	
1454		$CH_3\ as\ \delta, CH_2\ \varsigma$	$CH_3\ as\ \delta, CH_2\ \varsigma$
1393		$COO^-\ s\ \nu$	$COO^-\ s\ \nu$
1304		$Amide\ III$	
1247	$PO_2^-\ as\ \nu$		
1084	$PO_2^-\ s\ \nu$		

3.2 Irradiated sample

In figure 3 a comparison between the average control spectrum and the average spectra of samples exposed to different doses of X-rays, respectively equal to 2, 4, 6, 8, 10 Gy and fixed immediately after irradiation (X Gy; t = 0h) is reported. The obtained spectra show some differences in the relative intensity of the relative intensity of the absorption peaks.

There are differences in both high wavenumber and the fingerprint region, whose amplitudes increase at high dose. For high doses (8, 10 Gy) a change in the shape of the peak between 3300-3000 cm^{-1} as well as an increase in DNA-related peak centered at 1240 and 1090 cm^{-1} and the appearance of visible peaks structure below 1000 cm^{-1} for the 10 Gy spectrum associated with overlapping signals due to DNA, RNA, amino acids and carbohydrates [7], are visible.

Deconvolution of the spectra of the irradiated cells (not shown), in the region (3600-2000 cm^{-1}) and (2000-800 cm^{-1}), performed using the same procedures used for the control sample, show the same peaks of the control cells but with some shift in the position and intensity variations; as previously mentioned, a peaks structure centered at 880 cm^{-1} appears for the 10 Gy dose spectrum.

Shifts in the fingerprint region, are present at high doses (6, 8, 10 Gy) for amide II and carboxyl functional group (COO^-) peaks, respectively at 1522, 1553 and 1393 cm^{-1}, and for DNA peaks at 1084 cm^{-1} and 1247 cm^{-1}; those modification suggest conformational changes and/or rearrangement of existing proteins, lipids and nucleic acid structure. Moreover, shifts for the peak of amide A at 3293 cm^{-1} of the HWR are present, which evidence changes in the protein and amino acids structure.

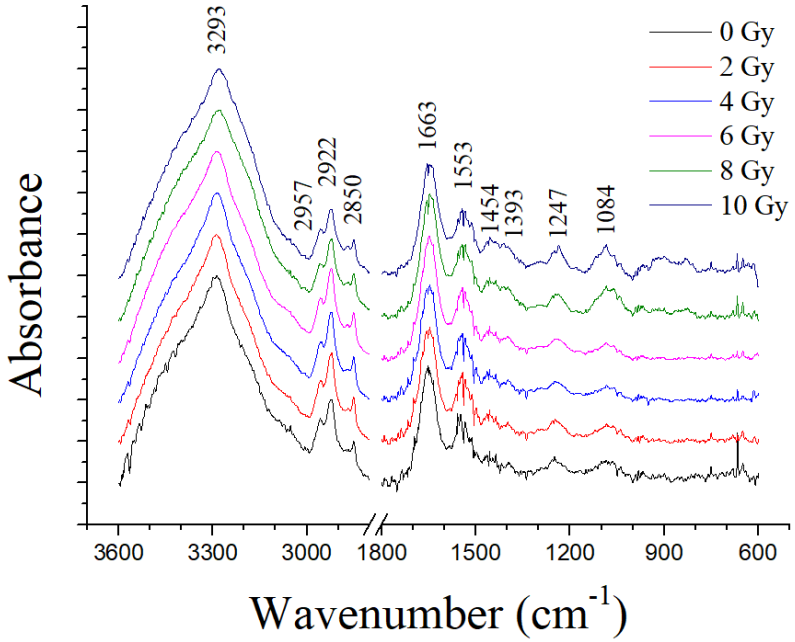

Figure 3. Comparison of average FTIR spectra in the region [3600 - 600 cm^{-1}] of the control cells (0 Gy; t = 0 h) and irradiated cells (2; 4; 6; 8; 10 Gy; t = 0 h); the spectra are shifted in absorbance to allow the comparison and present a break in free peaks region [2800 - 1800 cm^{-1}]; principal peak position, for the control sample are indicated.

To investigate the changes occurring in the secondary structure of protein the amide I region of control and irradiated samples fixed immediately after irradiation were analyzed; for all doses a deconvolution analysis of the peak in the spectral range (1720-1580 cm^{-1}) was performed using a Gaussian-Lorentzian cross product function. In figure 4, the deconvolution obtained for the average control spectrum is shown.

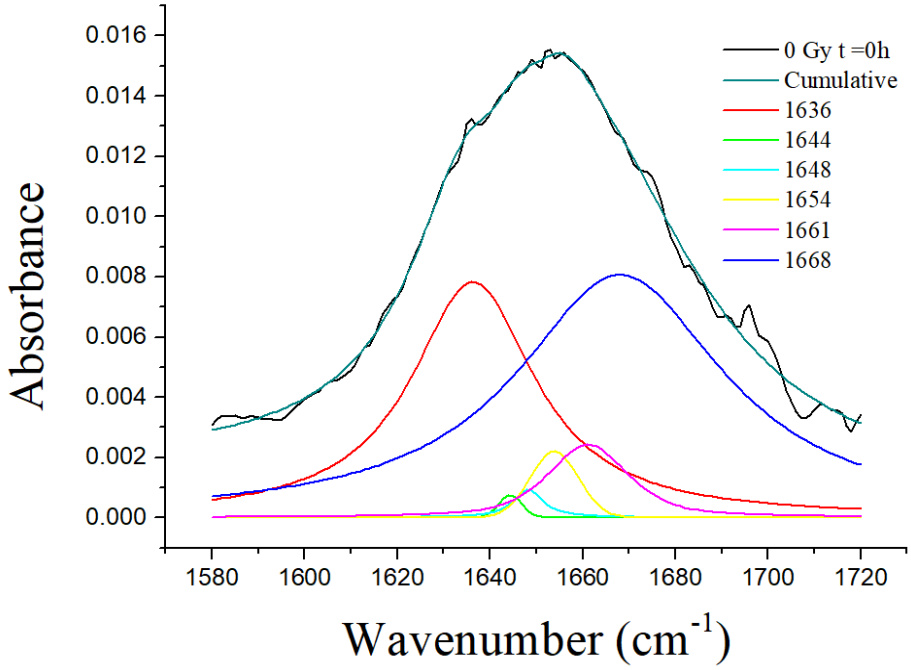

Figure 4. Average spectra of the control sample (0 Gy; t = 0 h) in the range [1720 - 1580 cm^{-1}] with deconvolution analysis of peaks with Gaussian - Lorentzian Cross Product curves.

In table 2 the deconvolution peaks position for control and irradiated samples with assignments in accordance with data in literature are reported, with the shifts of peak position compared to the control sample; the shifts with values greater of the spectra resolution of the instrument (4 cm^{-1}), are indicated in bold. For each peak, the amount of its area is reported as a percentage of the total area of cumulative peak.

Table 2. FTIR Amide I deconvolution peaks position for control and irradiated samples, fixed immediately after irradiation, with assignments in accordance with the data reported in the literature [15]. The shifts in terms of units of wavenumber are indicated in brackets (bold values stand for shifts greater than the spectral resolution of the instrument 4 cm^{-1}).

0 Gy	**Assignments**	**2 Gy**	**4 Gy**	**6 Gy**	**8 Gy**	**10 Gy**
Peak (cm^{-1})		Peak (cm^{-1})	Peak (cm^{-1})	Peak (cm^{-1})	Peak (cm^{-1})	Peak (cm^{-1})
1636	$\beta - sheets$	1639 (+3)	1636	1637 (+1)	1640 (+4)	1640 (+4)
% A = 36 ± 5		% A = 43 ± 6	% A = 13 ± 2	% A = 7.1 ± 0.7	% A = 16 ± 2	% A = 43 ± 6
1661	$\alpha - helix$	1659 (-2)	1656 (**-5**)	1659 (-2)	1657 (-4)	1657 (-4)
% A = 6.0 ± 0.9		% A = 43 ± 4	% A = 22	% A = 6.2 ± 0.8	% A = 11 ± 2	% A = 16 ± 2

Both β-sheets and α-helix components show changes with doses indicating a rearrangement in the secondary structure of protein content.
The same analysis was conducted on the spectra from non-irradiated and irradiated samples, fixed 24 hours after irradiation (X Gy; t = 24h). The average spectra obtained for all the doses are compared with the 0-dose spectrum in figure 5.

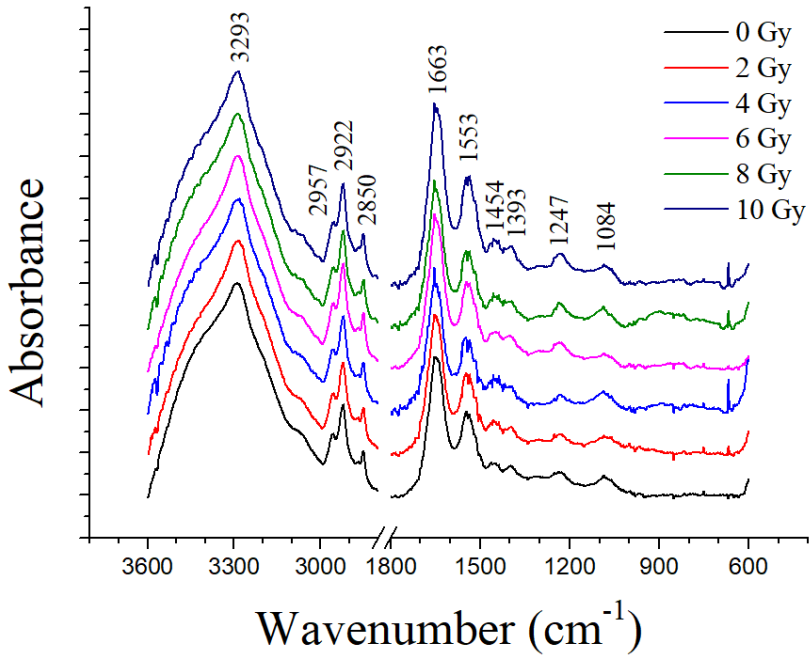

Figure 5. Comparison of average FTIR spectra in the region [3600 - 600 cm^{-1}] of the control cells (0 Gy; t = 24 h) and irradiated cells (2; 4; 6; 8; 10 Gy; t = 24 h); the spectra are shifted in absorbance to allow the comparison and present a break in free peaks region [2800 - 1800 cm^{-1}]; principal peak position, for the control sample are indicated.

The change in the absorbance appear smaller in respect of those found for the t_0-cells, especially at high doses (8, 10 Gy) where, only a pronounced peak, centered at 900 cm^{-1} (non-visible in the t_0 sample) appears. The spectrum at 10 Gy dose shows comparable differences in amplitude to those of the corresponding sample at t_0 only for the peaks of the amide I and II. These differences can be explained by the activation of cell repair process, during incubation. These processes can reduce radiation effects for the lowest doses while failing to do the same for high doses. Deconvolution of the spectra of the t24-samples, in the region (3600-2600 cm-1) and (2000-800 cm-1), are obtained (not

shown). They show the same peaks of the t0-cells with some shift in the position and intensity variations. The amide A peaks (at 3293 cm^{-1}) presents shifts at 4 and 8 Gy which always remain within the 4 cm^{-1} and show no dose dependent behavior, unlike from what was observed for the t_0-samples. In the fingerprint region, the sample at 4 Gy dose presents some significant shifts for the amide II peaks, 1553 and 1522 cm^{-1}, the peak at 1454 cm^{-1} and the peak at 1084 cm^{-1} that suggests conformational change for both proteins, lipids and nucleic acid structure at that dose. The amide III and the (PO^{-}_2) symmetric stretching of DNA bands, respectively at 1304 and 1084 cm^{-1} presents significant shifts for all dose above 2 Gy, with the peak of amide III that remains unresolved for the 4 Gy dose.

To investigate the changes occurring in the secondary structure of protein the amide I region of non-irradiated and irradiated samples fixed 24 h after irradiation were analyzed as previously described for t_0-samples. In table 3, the deconvolution peaks position for non-irradiated and irradiated samples with assignments in accordance with the data reported in the literature are reported, with the shifts of peak position compared to the control sample.

Table 3. FTIR Amide I deconvolution peaks position for control and irradiated samples, fixed 24 h after irradiation, with assignments in accordance with the data reported in the literature [50]. The shifts in terms of units of wavenumber are indicated in brackets (bold values stand for shifts greater than the spectral resolution of the instrument 4 cm^{-1}).

0 Gy	**Assignments**	**2 Gy**	**4 Gy**	**6 Gy**	**8 Gy**	**10 Gy**
Peak (cm^{-1})		Peak (cm^{-1})	Peak (cm^{-1})	Peak (cm^{-1})	Peak (cm^{-1})	Peak (cm^{-1})
1640	$\beta - sheets$	1638 (-2)	1639 (-1)	1639 (-1)	1640 (+4)	1637 (-3)
% A = 29 ± 3		% A = 12 ± 2	% A = 6.2 ± 0.7	% A = 72 ± 7	% A = 58 ± 6	% A = 72 ± 8
1666	$\alpha - helix$	1664 (-2)	1668 (+2)	1663 (-3)	unresolved	1664 (-2)
% A = 5.3 ± 0.6		% A = 79 ± 8	% A = 66 ± 7	% A = 4.1 ± 0.4		% A = 2.0 ± 0.2

Both β-sheets and α-helix components changes with doses. In particular, β-sheets decreases for 2 and 4 Gy and increases in a significant way from 6 to 10 Gy. α-helix has a discontinuous behavior with a significant increase for 2 and 4 Gy and a decrease for higher doses; this behavior can evidence the presence of unfolding processes.

4 CONCLUSIONS

The present work reports the preliminary results of an experimental investigation on X-rays induced variations on human neuroblastoma cells. The analysis of the irradiated samples fixed immediately after irradiation indicated significant differences with respect to spectrum of control cells. The deconvolution of the peaks of the spectra allow us to associate these variations to the relative biomolecule and to the relative molecular process such as the fragmentation of individual amino acids and DNA bases, the formation of molecular crosslinks that stiffen the structure of the DNA and the conformational change of proteins structure. The analysis of the irradiated samples fixed 24 h after irradiation was able to observe the expected reduction of radiation-induced damage as a consequence of cells repair mechanism. Further work is in progress in order to explore the possibility of using singular peaks area variations, with dose, as important biomarkers of radiation damage.

REFERENCES

[1] Gault, N., Lefaix, J.L., “Infrared microspectroscopic characteristics of radiation-induced apoptosis in human lymphocytes”, Radiation research 160, 2, 238-250 (2003).

[2] Gasparri, F., Muzio, M., “Monitoring of apoptosis of hl60 cells by Fourier-transform infrared spectroscopy”, Biochemical Journal 369, 2, 239-248 (2003)

[3] Krishna, C.M., Kegelaer, G., Adt, I., Rubin, S., Kartha, V., Manfait, M., Sockalingum, G., “Characterization of uterine sarcoma cell lines exhibiting mdr phenotype by vibrational spectroscopy”, Biochimica et Biophysica Acta (BBA)-General Subjects 1726, 2, 160-167 (2005)

[4] Mourant, J.R., Short, K.W., Carpenter, S., Kunapareddy, N., Coburn, L., Powers, T.M., Freyer, J.P., “Biochemical differences in tumorigenic and nontumorigenic cells measured by Raman and infrared spectroscopy, Journal of Biomedical Optics 10, 3, 031106 (2005)

[5] Delfino, I., Perna, G., Ricciardi, V., Lasalvia, M., Manti, L., Capozzi, V., Lepore, M., "X-ray irradiation effects on nuclear and membrane regions of single SH-SY5Y human neuroblastoma cells investigated by Raman micro-spectroscopy", Journal of Pharmaceutical and Biomedical Analysis, 164, 557-573 (2019)
[6] Baker, M.J., Trevisan, J., Bassan, P., Bhargava, R., Butler, H.J., Dorling, K.M., Fielden, P.R., Fogarty, S.W. Fullwood, N.J. Heys, K.A. "Using Fourier transform IR spectroscopy to analyze biological materials", Nat. Protoc. 9, 1771–1791 (2014)
[7] Meade, A., Clarke, C., Byrne, H., Lyng, F., "Fourier transform infrared microspectroscopy and multivariate methods for radiobiological dosimetry", Radiation research 173 (2), 225-237 (2010)
[8] Gianoncelli, A., Vaccari, L., Kourousias, G., Cassese, D., Bedolla, D. E., Kenig, S., Storici, P., Lazzarino, M., Kiskinova, M., "Soft X-ray microscopy radiation damage on fixed cells investigated with synchrotron radiation FTIR microscopy", Sci. Rep. 5, 10250 (2015).
[9] Encinas M., Iglesias, M., Liu, Y., Wang, H., Muhaisen, A., Ceña, V., Gallego, C., Comella, J.X. "Sequential treatment of SH-SY5Y cells with retinoic acid and brain-derived neurotrophic factor gives rise to fully differentiated, neurotrophic factor-dependent, human neuron-like cells", J Neurochem, 75, 991–1003 (2000)
[10] Koriyama, Y., Furukawa, A., Muramatsu, M., Takino, J., Takeuchi, M., "Glyceraldehyde caused Alzheimer's disease-like alterations in diagnostic marker levels in SH-SY5Y human neuroblastoma cells", Sci Rep, 5, 13313 (2015)
[11] Mei, Y., Miller, L., Gao, W., Gross, R.A., "Imaging the distribution and secondary structure of immobilized enzymes using infrared microspectroscopy", Biomacromolecules, 4, 70-74 (2003)
[12] Delfino, I., Portaccio, M., Della Ventura, B., Mita, D.G., Lepore, M., "Enzyme distribution and secondary structure of sol-gel immobilized glucose oxidase by microattenuated total reflection FT-IR spectroscopy", Mater. Sci. Eng. C, 33, 304-301.5 (2013)
[13] Ricciardi, V., Portaccio, M., Piccolella, S., Manti, L., Pacifico, S., Lepore, M., "Study of SH-SY5Y cancer cell response to treatment with polyphenol extracts using FT-IR Spectroscopy", Biosensors, 7, 57 (2017); doi:10.3390/bios7040057
[14] Meade, A.D., Lyng, F.M., Knief, P., Byrne, H.J., "Growth substrate induced functional changes elucidated by ftir and Raman spectroscopy in in-vitro cultured human keratinocytes", Analytical and Bioanalytical Chemistry 387, 5, 1717–1728 (2007)
[15] Barth, A., "Infrared spectroscopy of proteins", Biochimica et Biophysica Acta (BBA)-Bioenergetics 1767, 9, 1073-1101 (2007)
[16] Gault, N., Rigaud, O., Poncy, J.L., Lefaix, J.L., "Infrared microspectroscopy study of γ-irradiated and H_2O_2 - treated human cells", Int. J. Radiat. Biol. 81, 10, 767-779 (2005)